Check for updates

Original Article

Newly Generated 3D Schwann-Like Cell Spheroids From Human Adipose-Derived Stem Cells Using a Modified Protocol

Cell Transplantation
Volume 31: 1–9
© The Author(s) 2022
Article reuse guidelines:
sagepub.com/journals-permissions
DOI: 10.1177/09636897221093312
journals.sagepub.com/home/cll
SAGE

Shuhai Chen[1], Tetsuya Ikemoto[1], Takuya Tokunaga[1], Shouhei Okikawa[1], Katsuki Miyazaki[1], Shinichiro Yamada[1], Yu Saito[1], Yuji Morine[1], and Mitsuo Shimada[1]

Abstract

Peripheral nerve injury (PNI) is a relatively frequent type of trauma that results in the suffering of many patients worldwide every year. Schwann cells (SCs) are expected to be applied in cell therapy because of their ability to promote peripheral nerve regeneration. However, the lack of clinically renewable sources of SCs hinders the application of SC-based therapies. Adipose-derived stem cells (ADSCs) have generated great interest in recent years because of their multipotency and ease of harvest, and they have already been verified to differentiate into Schwann-like cells (SLCs) in vitro. However, the efficiency of differentiation and the functions of SLCs remain unsatisfactory. We newly generated three-dimensional (3D) SLC spheroids from ADSCs using a modified protocol with human recombinant peptide (RCP) petaloid μ-piece. Morphological analysis, gene expression analysis by qRT-PCR, ELISA measurement of the secretion capabilities of neurotrophic factors, and neurite formation assay were performed to evaluate the functions of these 3D SLCs in vitro. Motor function recovery was measured in a sciatic nerve injury mouse model to analyze the nerve regeneration-promoting effect of 3D SLCs in vivo. The differentiation efficiency and the secretion of neurotrophic factors were enhanced in 3D SLCs compared with conventional SLCs. 3D SLCs could more effectively promote neurite growth and longer neurite extension in a neuron-like SH-SY5Y model. Additionally, 3D SLCs had a better therapeutic effect on nerve regeneration after transplantation into the sciatic nerve injury mouse model. These findings demonstrated that the potential of ADSC-derived SLCs to promote nerve regeneration could be significantly increased using our modified differentiation protocol and by assembling cells into a 3D sphere conformation. Therefore, these cells have great potential and can be used in the clinical treatment of PNI.

Keywords

Schwann-like cells, adipose-derived stem cells, three-dimensional model, nerve regeneration

Introduction

Peripheral nerve injury (PNI) is a relatively frequent type of trauma that affects more than 1 million people worldwide every year and is a global clinical problem that exhibits a significant socioeconomic burden[1]. Autologous nerve anastomosis is considered the gold standard for PNI treatment[2]. However, because of the need to sacrifice naive nerve tissues, the risk of neuroma formation, and other complications associated with this second surgery, its application is limited[3,4]. In addition, PNI caused by pelvic surgery must be addressed to improve patients' quality of life[5]. Cell therapy based on Schwann cells (SCs) may be a good option because the mechanism is ideal. Previous reports demonstrated that SCs could accelerate peripheral nerve repair through a variety of mechanisms, including establishment of a regeneration guide, secretion of neurotrophic factors, and remyelination of damaged axons[6–9]. However, because of limitations regarding the isolation, purification, and proliferation technology of primary SCs, there is an urgent need to develop a method to generate large numbers of replacement cells with low immunogenicity[10]. Our previous studies have successfully demonstrated a modified protocol to effectively induce Schwann-like cells (SLCs) from adipose-derived stem cells (ADSCs) into an SC

[1] Department of Digestive and Transplant Surgery, Tokushima University, Tokushima, Japan

Submitted: January 15, 2022. Revised: March 11, 2022. Accepted: March 23, 2022.

Corresponding Author:
Tetsuya Ikemoto, Department of Digestive and Transplant Surgery, Tokushima University, 3-18-15 Kuramoto, Tokushima 770-8503, Japan.
Email: ikemoto.tetsuya@tokushima-u.ac.jp

Creative Commons Non Commercial CC BY-NC: This article is distributed under the terms of the Creative Commons Attribution-NonCommercial 4.0 License (https://creativecommons.org/licenses/by-nc/4.0/) which permits non-commercial use, reproduction and distribution of the work without further permission provided the original work is attributed as specified on the SAGE and Open Access pages (https://us.sagepub.com/en-us/nam/open-access-at-sage).

phenotype with typical repair characteristics and increased secretion of nerve growth factor (NGF)[11].

However, other important issues still need to be addressed, such as improving cell viability and differentiation efficiency and increasing the retention and survival of cells after transplantation[10,12]. In the traditional two-dimensional cell culture method, cells are in a single-layer structure, and the interactions between the cells do not reflect those in physiological tissues. In addition, adherent cells need to be treated with trypsin before transplantation to produce a single cell suspension, which inevitably disrupts the cell–cell interactions and the extracellular matrix (ECM) of the cells. This process causes cell destruction before transplantation, thus greatly reducing the cell function and their subsequent therapeutic potential[13,14]. Culturing cells in a three-dimensional (3D) sphere configuration can promote the differentiation efficiency of stem cells and improve the final therapeutic efficacy of cell transplantation and cell therapy and is widely used in tissue engineering[15–17]. We previously established and reported the generation of effective insulin-producing cells from ADSCs and examined their advantages in vitro and in vivo, and these cells will soon be used in the first in-human clinical trials[18–22]. These cells were generated using a human recombinant peptide (RCP) petaloid μ-piece provided by Fuji Film (Tokyo, Japan). The RCP μ-piece acts as a scaffold for ADSCs and can support the formation of a large cell cluster. The features of this RCP include xeno-antigen-free characteristics, high cell adhesiveness, biodegradation absorption, clinical-grade quality, and stable manufacturing quality[23]. Therefore, it can achieve a cell aggregate-like technology. The generated large cell cluster is named as "CellSaic" because the cells and RCP petaloid μ-piece are combined like a mosaic. This CellSaic is able to form a 3D sphere and maintain the viability of transplanted cells[24]. Therefore, we adapted this technique for SLC differentiation.

Here, we report our establishment of 3D SLC spheroids from ADSCs using our modified protocol with an RCP μ-piece. We also demonstrate their enhanced therapeutic potential for peripheral nerve regeneration both in vitro and in vivo.

Materials and Methods

Cell Culture and Preparation of ADSC-Derived SLCs

Human ADSCs were purchased from Invitrogen (Grand Island, NY, USA) and maintained in ADSC basal medium with added growth supplement (Gibco, Carlsbad, CA, USA) and GlutaMAX-I (Gibco). Primary human SCs were procured from ScienCell Research Laboratories (Carlsbad, CA, USA) and cultured in complete SC medium (ScienCell Research Laboratories) according to the manufacturer's instructions. The SH-SY5Y cell line was obtained from ATCC (CRL-2266, Manassas, VA, USA) and maintained in DMEM/F12 (Thermo Fisher Scientific, Inc. Waltham, MA, USA) supplemented with 15% fetal bovine serum (FBS) (Thermo Fisher Scientific, Inc.) and a 1% penicillin-streptomycin solution (Thermo Fisher Scientific, Inc.). To induce differentiation of ADSCs into SLCs, ADSCs were cultured for three to five passages, and then 1×10^5 ADSCs/well were seeded onto collagen I-coated six-well plates (4810-010; IWAKI, Tokyo, Japan) for the conventional SLC group, or 2×10^4 ADSCs/well mixed with 0.2 mg/ml μ-piece (16629004; Fuji Film) were seeded onto ultra-low attachment 96-well plates (174925; Thermo Fisher Scientific) for the 3D SLC group. After cells in the 3D group had formed a spheroid in each well (approximately 24 h after seeding), our modified protocol with folic acid[11] was used to induce differentiation in both the conventional SLC and 3D SLC groups. All cells were incubated at 37 °C with 5% CO_2 in a humidified incubator. When the medium was changed, 2 ml/well medium was added to the conventional SLC group and 100 μl/well was added to the 3D SLC group.

Morphological Analysis of 3D Spheroids

During differentiation, the morphology of 3D spheroids was directly observed, and images were captured by a light microscope (magnification, ×100; DP22-CU; Olympus, Tokyo, Japan). For microtomy, spheres were solidified using iPGell (PG20-1; Genostaff, Osaka, Japan) and fixed in 4% paraformaldehyde, as previously described[25]. After embedding in paraffin and slicing at a thickness of 5 μm, hematoxylin and eosin staining was performed according to a standard protocol.

Quantitative Real-Time Reverse Transcription Polymerase Chain Reaction (qRT-PCR)

An RNeasy Mini Kit (Qiagen, Hilden, Germany) was used to extract the total RNA in each sample according to the manufacturer's instructions. After measurement of the RNA concentration using a spectrophotometer (NanoDrop 2000; Thermo Fisher Scientific), 2.5 μg RNA was reverse-transcribed into cDNA using a reverse transcription kit (Applied Biosystems, Thermo Fisher Scientific) in a total of 50 μl of the reaction system, in accordance with the manufacturer's instructions. The StepOnePlus Real-Time PCR System (Applied Biosystems, Thermo Fisher Scientific, Inc.) was used to perform TaqMan-qRT-PCR analyses under the following thermocycling conditions: initial denaturation at 95 °C for 3 min; 40 cycles of denaturation at 95 °C for 30 s, annealing at 58 °C for 30 s, and extension at 72 °C for 45 s; and final extension at 72 °C for 10 min. The primers (TaqMan gene expression assays; Thermo Fisher Scientific) were *S100B* (Hs00902901_m1) and *NGFR* (Hs00609976_m1). Glyceraldehyde 3-phosphate dehydrogenase (*GAPDH*; 4326317E) was used as the internal control, and the results were expressed as the relative mRNA expression change in the experimental group compared with the control group.

Enzyme-Linked Immunosorbent Assay (ELISA)

After washing twice with phosphate-buffered saline (PBS), serum-free DMEM was added to the indicated cells. The supernatant was collected after 48 h of incubation, centrifuged (500 × g; 20 min) at room temperature, and filtered using a 0.2 μm filter to remove the cell debris. The cells were digested with trypsin and re-counted. Next, Human NGF ELISA kit (BEK-2212-1P; Biosensis, Thebarton, Australia) and Human Glial Cell-Derived Neurotrophic Factor (GDNF) ELISA kit (BEK-2222-1P; Biosensis) were used to assess NGF and GDNF secretion in supernatants according to the manufacturer's instructions. The absorbance was measured at 450 nm (540 nm as the reference wavelength) using a microplate reader (SpectraMax i3; Molecular Devices, CA, USA). The relative secretion capacity was normalized to the cell number.

Immunofluorescence Staining

Cells were mounted on slides, washed twice with PBS, and fixed with 4% paraformaldehyde (163-20145; FUJIFILM) at 4 °C for 30 min. For frozen sections, slides were reheated and dried at room temperature for 30 min and then washed in PBS for 5 min to remove the residual O.C.T. Compound (4583; Sakura Finetek Japan Co., Ltd., Tokyo, Japan). After permeabilization with 0.1% Triton X-100 (HFH10; Thermo Fisher Scientific) for 5 min at room temperature, all slides were incubated with 3% bovine serum albumin (BSA) diluted from MACS BSA Stock Solution (130-091-376; Miltenyibiotec, Bergisch Gladbach, Germany) in PBS for 60 min at room temperature. Then, the slides were incubated with an anti-βIII tubulin antibody (ab18207, 1:500; Abcam, Cambridge, UK) at 4 °C overnight. The next day, the slides were washed three times with PBS and incubated with Alexa Fluor 488-conjugated secondary antibodies (A-11008, 1:1000; Thermo Fisher Scientific, Inc.) for 1 h at 37 °C in the dark. After three washes with PBS in the dark, ProLong Gold Antifade Mountant with DAPI (P36931; Thermo Fisher Scientific) was used to stain the nuclei for 10 min in the dark. The slides were observed and photographed under a fluorescence microscope (BZ-X700; KEYENCE, Tokyo, Japan). For negative controls, the primary antibody was replaced with BSA.

In Vitro Effects of SLCs on Neurite Formation in Neural Cells

To induce a neuronal-like phenotype, SH-SY5Y cells were stimulated in DMEM/F12 supplemented with 1% FBS and 10 μM retinoic acid (Sigma–Aldrich, St Louis, MO, USA) for 5 days according to previous reports[16,26,27], and then seeded on the Nunc Lab-Tek II Chamber Slide system (Cat. No. 154526PK; Thermo Fisher Scientific). ADSCs, conventional SLCs, and 3D SLCs were seeded (6×10^5 cells/well) in an insert (Falcon Permeable Support for a 24-well Plate with a 0.4 μm Transparent PET Membrane, 353095; Corning, NY, USA) and co-cultured with SH-SY5Y cells for 48 h in an indirect contact manner, which involved sharing the same medium with SH-SY5Y cells. For the control group, SH-SY5Y cells were cultured alone. After co-cultivation, the slides were washed three times with PBS, and then immunofluorescence staining was performed as described above. ImageJ v1.46r software (National Institute of Mental Health, Bethesda, MD, USA) with the NeurphologyJ plugin was used to analyze the immunofluorescence staining images, and the number of branching neurites and neurite length of each neuron were calculated. According to previous reports[16,28], this software is capable of automatically quantifying neuronal morphologies such as the number of branching neurites, neurite length, and neurite branching complexity, and it has been verified and applied in previous experiments in SCs. The results are expressed as the relative length in the experimental group compared with the control group.

In Vivo Sciatic Nerve Injury Model and Cell Transplantation

Male BALB/c nu-nu nude mice at 8 weeks of age were supplied by CIEA, JAC Inc. (Tokyo, Japan) and bred at the animal facility of Tokushima University for all experiments. After mice were anesthetized with isoflurane and the local skin was disinfected, a 1 cm incision was made in the right hind limb, and the biceps femoris muscle was bluntly separated to expose the right sciatic nerve. The nerve was injured by cutting the central region as previously described[29], and cell transplantation was performed immediately. ADSCs and conventional SLCs were digested with trypsin and suspended in PBS. For 3D SLCs, spheroids (2×10^4 cells/spheroid) were collected by pipette tip and gently washed twice with PBS. Then, a total of 1×10^6 cells in 100 μl PBS or PBS alone (control group) were directly administered to the site of the nerve defect of one mouse in each group. The wound was sutured, and footprint analysis was performed weekly until the animals were killed. The experiments and procedures were approved by the Animal Care and Use Committee of the University of Tokushima.

Sciatic Function Index (SFI) Analysis

Quantitative in vivo functional recovery was evaluated postoperatively using footprint analysis and the SFI[30]. Briefly, the hind paws of mice were painted with red ink, and the mice were allowed to walk down a white paper-covered track (length 50 cm, width 6 cm) at 1, 2, 3, and 4 weeks after the surgery. Three mice in each group were assessed, and each mouse walked along the track three times. The hind paw prints were scanned, and the print length (PL, distance between the heel and the third toe), toe spread (TS, distance

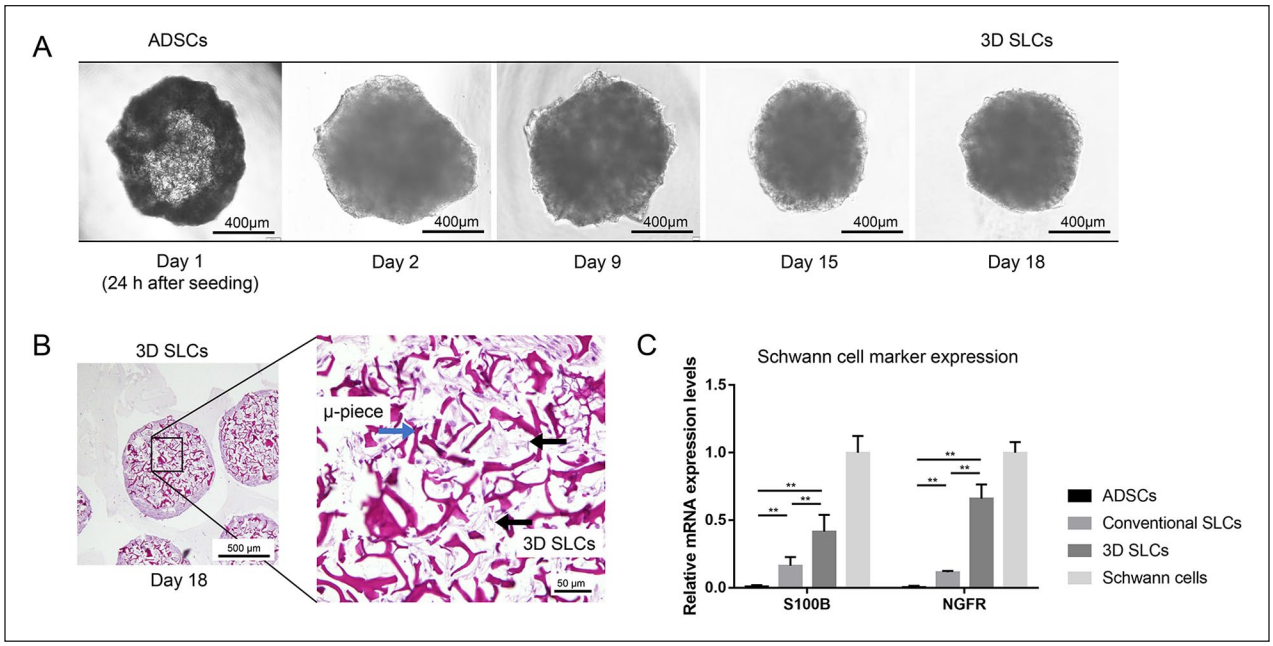

Figure 1. Three-dimensional (3D) SLC spheroids generated from ADSCs. (A) Representative image of cell morphology under light microscopy during the differentiation process. (B) The morphology of 3D SLC spheroids is shown after hematoxylin and eosin staining. (C) Gene expression levels of the Schwann cell markers *S100B* and *NGFR* were detected in ADSCs, conventional SLCs, 3D SLCs, and primary Schwann cells using RT-qPCR analysis (n = 4). Data are expressed as means ± SD. $^{**}P < 0.01$, one-way ANOVA with Tukey's post-test. Scale bar in A, 400 μm; B (left), 500 μm; B (right), 50 μm. ADSCs: Adipose-derived stem cells; *NGFR*: nerve growth factor receptor; SLC: Schwann-like cell; *S100B*: S100 calcium-binding protein B.

between the first and the fifth toe), and intermediary toe spread (IT, distance between the second and the fourth toe) were measured to calculate the SFI using the following formula: SFI = −38.3 × (EPL−NPL)/NPL + 109.5 × (ETS−NTS)/NTS + 13.3 × (EIT−NIT)/NIT−8.8 (E, experimental foot; N normal foot)[29].

Euthanasia and Harvesting of Tissue Specimens From Mice

After each mouse was killed, the gastrocnemius muscle of the injured limb was separated carefully and weighed immediately. The relative wet weights of gastrocnemius muscles were obtained by dividing by the corresponding bodyweight of the mouse. The sciatic nerve containing the regenerated portion was carefully isolated, embedded in O.C.T. compound, and immediately frozen in liquid nitrogen. Cryostat sections (5 μm) were mounted on glass slides and stored at −80 °C until immunofluorescence staining was performed.

Statistical Analysis

Data are expressed as the mean ± standard deviation. Statistical analysis and graph plotting were performed with GraphPad Prism 7.0 software (GraphPad Software, Inc. San Diego, CA, USA) and ImageJ v1.46r software. One-way analysis of variance (ANOVA) or two-way ANOVA with Tukey's test was used to compare differences among multiple groups. All experiments were repeated at least three times. A p-value of 0.05 was considered to indicate statistical significance.

Results

Characteristics of SLCs Generated Using the 3D Culture System

Human ADSCs were differentiated into SLCs using our protocol according to our previous report[11]. Representative images show the morphological changes in the 3D SLC group during the differentiation process (Fig. 1A). After 18 days of differentiation, the cells aggregated into a tight spheroid with a slightly reduced volume. Adequate cell formation was maintained using the RCP μ-piece as a scaffold, as shown in Fig. 1B. Moreover, the expression of SC markers such as S100 calcium-binding protein B (*S100B*) and nerve growth factor receptor (*NGFR*) was significantly upregulated in 3D SLCs compared with conventional SLCs, which demonstrated that the differentiation efficiency was improved using the 3D culture system (Fig. 1C).

3D SLCs Exhibited Enhanced Therapeutic Potential In vitro

In the in vitro functional evaluation, we examined the ability of SLCs to secrete neurotrophic factors and whether they

could promote neurite outgrowth in neurons. NGF and GDNF secretion were significantly upregulated in both conventional SLCs and 3D SLCs compared with ADSCs. However, the 3D SLC group had a greater secretion capacity (Fig. 2A, B). Immunofluorescence staining of βIII tubulin was used to estimate the number and length of neurites. After direct co-culture with SLCs, the neurite outgrowth of SH-SY5Y cells was significantly enhanced (Fig. 2C). The statistical results revealed significantly more neurite branching. Moreover, longer neurite extensions in SH-SY5Y cells were observed in the 3D SLC group after calculation via the NeurphologyJ plugin. All these observations confirmed the superiority of 3D SLCs over conventional SLCs and undifferentiated ADSCs (Fig. 2D, E).

3D SLCs Promoted Motor Function and Structural Recovery in a Sciatic Nerve Injury Model

Next, we investigated the in vivo effect of 3D SLCs in a sciatic nerve injury nude mouse model. Immediately after injury, ADSCs, conventional SLCs, and 3D SLCs were transplanted into the injured area according to a previous report[28], and motor functional recovery of the injured sciatic nerve was evaluated by footprint analysis. Representative walking footprints of mice from each group at 4 weeks after cell engraftment are shown in Fig. 3A. At day 7, footprint analysis showed that there were no statistically significant differences in the SFI among all groups. At 28 days after transplantation, the 3D SLC group demonstrated better motor function than both the conventional group and the ADSC group, as revealed by the highest SFI value and the greatest SFI improvement in the 3D SLC group (Fig. 3B, C). Moreover, we analyzed the gastrocnemius muscle weight in the injured limbs of each group because denervation could induce muscle atrophy. The relative weights of gastrocnemius muscles were highest in the 3D SLC group, which confirmed the ability of 3D SLCs to promote nerve regeneration after injury (Fig. 3D, E). Finally, the injured nerve was observed, which showed some fibrous tissue connections in damaged nerves (Fig. 3F). Furthermore, βIII tubulin immunofluorescence staining showed incomplete nerve regeneration (Fig. 3G).

Discussion

We differentiated ADSCs into 3D SLC spheroids using a modified protocol with an RCP μ-piece for PNI treatment. The enhanced protocol uses non-gene editing methods, and its advantages include its ability to induce ADSCs to an SC phenotype with typical repair characteristics and increase NGF secretion[11]. In addition, 3D SLC spheroids exhibited enhanced therapeutic potential both in vitro and after transplantation into a murine sciatic nerve injury model.

Morphological observations showed that SLCs and the μ-piece formed a “CellSaic” in the 3D spheroids. This structure has been reported to effectively promote cell survival after transplantation[31]. The mRNA expression levels of the most commonly used mature SC markers, S100 and NGFR[27,32], were significantly higher in 3D SLCs than in conventional SLCs, indicating their greater differentiation efficiency. This advantage is produced by the 3D culture system, which more accurately reflects physiological conditions[18].

Paracrine secretion of neurotrophic factors by SLCs is an important mechanism for promoting nerve regeneration, and NGF and GDNF are the two most important factors[8,33]. We assessed the secretion of these factors using an ELISA, and our results showed that 3D SLCs exhibited greater secretion ability. To further determine whether 3D SLCs can functionally support neurite formation, we used a neuron-like human cell line, SH-SY5Y, which was induced by retinoic acid as a model to evaluate the potential of SLCs to promote axon growth[16,26,27]. By labeling βIII tubulin, which is a neuron-specific protein, immunofluorescence staining was used to visualize the neurites[16]. In the co-cultivation experiment, both conventional SLCs and 3D SLCs showed high therapeutic potential for promoting neurite growth. Upon interaction with SH-SY5Y cells, the 3D SLC group promoted increases in the number and length of neurites, which indicated that 3D SLCs were beneficial for neuron growth.

To further verify the function of 3D SLCs, a widely used sciatic nerve injury model was used to explore their effect on PNI repair in vivo[29,34]. The results showed that ADSC, conventional SLC, and 3D SLC transplantation could improve the SFI and prevent denervation-induced gastrocnemius muscle atrophy. Consistent with the in vitro experiments, the 3D SLC group exhibited an enhanced ability to promote nerve repair after transplantation. In addition to the greater differentiation efficiency and secretion capacity of 3D SLCs confirmed by the above in vitro experiments, the multicellular 3D spheroids retained their cell–cell and cell–ECM interactions, whereas conventional SLCs require trypsin digestion when preparing cell suspensions for transplantation. The ECM has been shown to effectively store growth factors secreted from cells[35] and enhance cell adhesion and survival after transplantation[18,36]. Moreover, human pluripotent stem cells (i.e., ES cells and iPS cells) have potential risks of tumorigenicity[37] in clinical applications compared with our SLCs. Considering other cell types, we have already demonstrated that matured cells differentiated from ADSCs have low risks of tumorigeneicity[18]. Therefore, consistent with previous studies[16,36,38,39], the therapeutic cells delivered by the 3D spheroids in our study showed better therapeutic potential.

Although we successfully generated 3D SLC spheroids with enhanced therapeutic ability, this study still has some limitations. The current differentiation period is 18 days, which is relatively long. Because attempts to shorten the differentiation time have not been successful[40], additional studies should be conducted to develop a shorter and more economical differentiation protocol. Moreover, even though we demonstrated that the regenerative ability of our 3D SLCs was significantly superior to that of ADSC administration alone, the efficiency of nerve regeneration is still not sufficient because only an incomplete connection of the injured

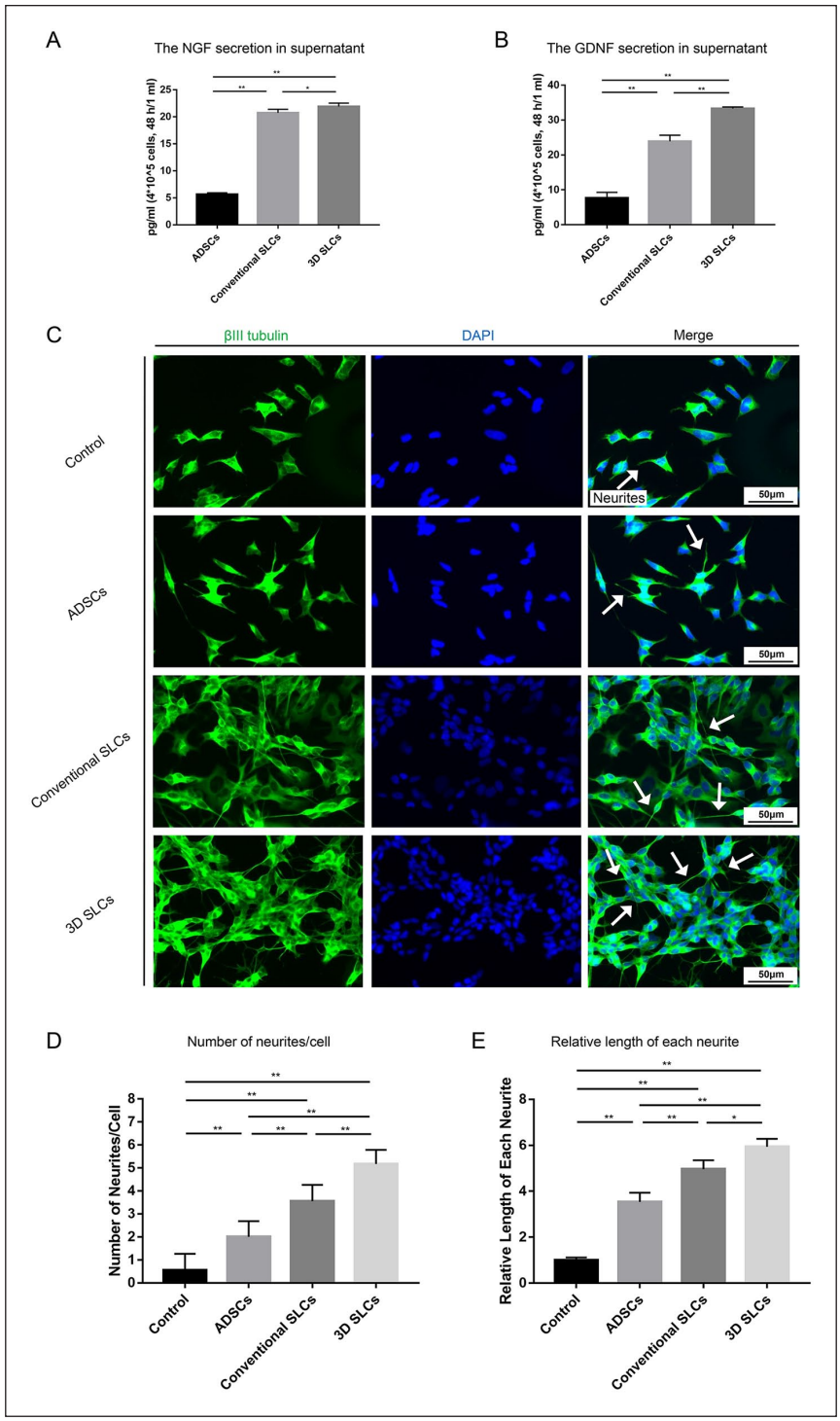

Figure 2. Three-dimensional (3D) SLCs exhibit enhanced therapeutic potential in vitro. The relative secretion of NGF (A) and GDNF (B) in the supernatant was analyzed by an enzyme-linked immunosorbent assay in the ADSC, conventional SLC, and 3D SLC groups (n = 4). Data are expressed as means ± SD. *$P < 0.05$; **$P < 0.01$, one-way ANOVA with Tukey's post-test. (C) Representative images of SH-SY5Y cells after direct co-culture with ADSCs, conventional SLCs, and 3D SLCs. The neurites were visualized by immunofluorescent labeling of βIII tubulin (green). (D) Statistical analyses of the number of neurites per cell (n = 4). Data are expressed as means ± SD. *$P < 0.05$; **$P < 0.01$, one-way ANOVA with Tukey's post-test. (E) Statistical analyses of the relative length of each neurite (n = 4). Data are expressed as means ± SD. *$P < 0.05$; **$P < 0.01$, one-way ANOVA with Tukey's post-test. Scale bar in C, 50 μm. SLCs: Schwann-like cells; NGF: nerve growth factor; GDNF: glial cell-derived neurotrophic factor; ADSC: Adipose-derived stem cell; DAPI, 4,'6-diamidino-2-phenylindole, dihydrochloride.

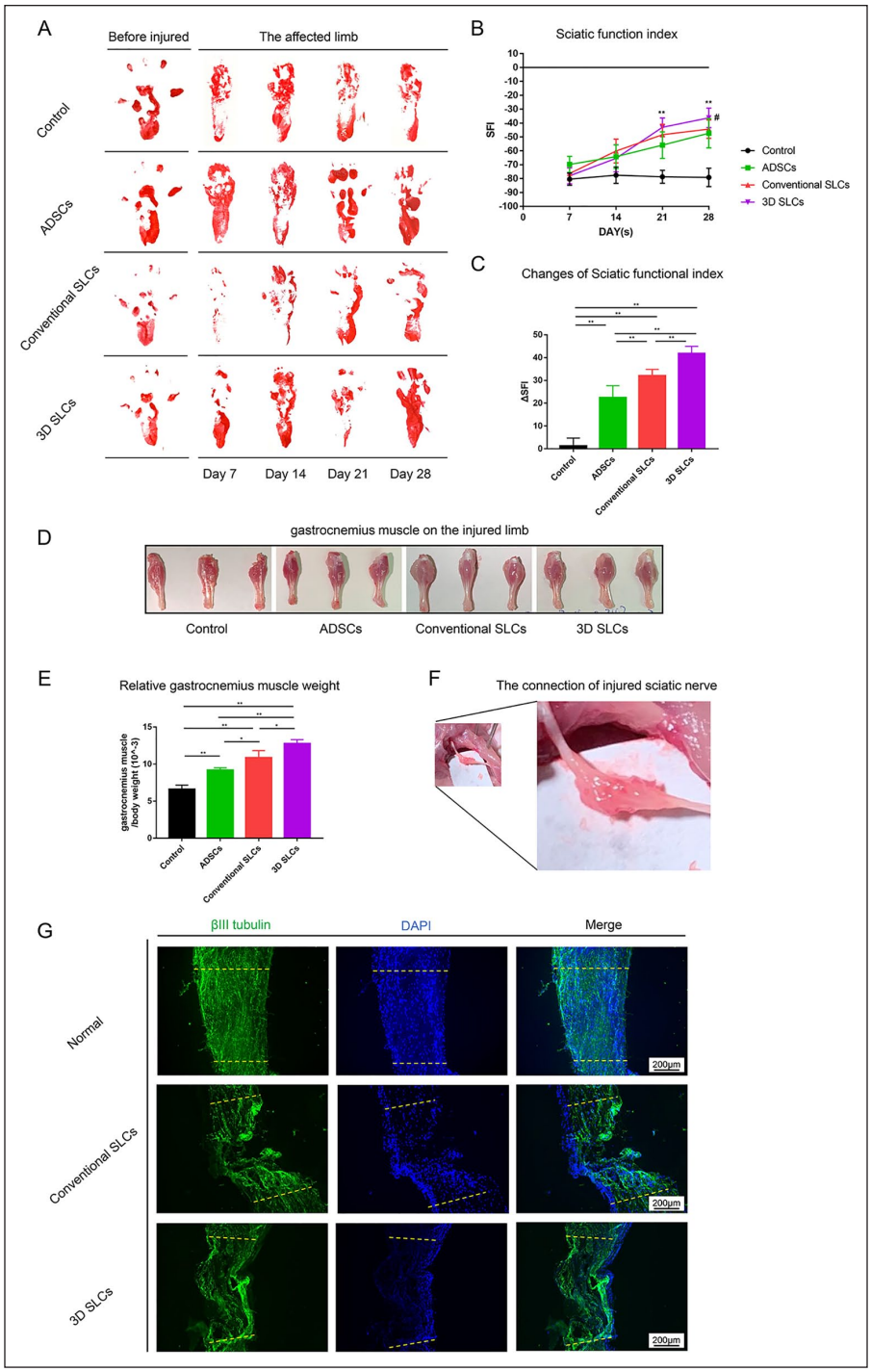

Figure 3. Three-dimensional (3D) SLCs promote motor function and structural recovery in vivo. (A) Representative images of the right hind paw prints of the control, ADSC, conventional SLC, and 3D SLC groups before injury and 1, 2, 3, and 4 weeks after injury. (B) Change in the SFI from 1 week to 4 weeks after injury (n = 3). Data are expressed as means ± SD. *$P < 0.05$ vs. control; **$P < 0.01$ vs. control; ##p < 0.01 vs. conventional SLCs, two-way ANOVA with Tukey's post-test. (C) Statistical analyses of the differences between 1 week and 4 weeks post-surgery (n = 3). Data are expressed as means ± SD. **$P < 0.01$, one-way ANOVA with Tukey's post-test. (D) Representative images of the gastrocnemius muscle of the injured limb in the control, ADSC, conventional SLC, and 3D SLC groups at 4 weeks post-surgery. (E) The relative weights of gastrocnemius muscles in the control, ADSC, conventional SLC, and 3D SLC groups at 4 weeks post-surgery (n = 3). Data are expressed as means ± SD. *$P < 0.05$; **$P < 0.01$, one-way ANOVA with Tukey's post-test. (F) Representative image of sciatic nerve regeneration after 3D SLC transplantation into the injured nerve region for 4 weeks. (G) βIII tubulin (green) expression was determined by immunofluorescence staining in the regenerated sciatic nerve. The dotted lines indicate the borders of injury sites. Scale bar in G, 200 μm. SLCs: Schwann-like cells; ADSC: Adipose-derived stem cell; SFI: Sciatic Function Index; DAPI, 4,'6-diamidino-2-phenylindole, dihydrochloride.

nerve was observed. Especially in large nerve defects, guidance for nerve stump growth is lacking, which prompted us to further combine the cells with more structurally supportive biomaterials such as a conduit[34]. Furthermore, the fate of transplanted SLCs remains unknown. Many transplanted animals are required for this cell tracking system because in vivo closed circumstances might be desirable for nerve regeneration. Thus, cell tracking experiments will be conducted in the future to reveal the mechanism of the acceleration of peripheral nerve regeneration using our 3D SLCs.

Conclusion

The results of this study demonstrate the feasibility of 3D SLC spheroids generated through a modified differentiation protocol combined with an RCP μ-piece as an alternative cell source to promote peripheral nerve regeneration. In vitro and in vivo experiments showed that the cells exhibited significantly improved therapeutic potential. This method may have great potential for clinical application in PNI treatment.

Abbreviations

ADSCs, adipose-derived stem cells; BSA, bovine serum albumin; DAPI, 4',6-diamidino-2-phenylindole, dihydrochloride; ECM, extracellular matrix; ELISA, enzyme-linked immunosorbent assay; FBS, fetal bovine serum; GDNF, glial cell-derived neurotrophic factor; NGF, nerve growth factor; NGFR, nerve growth factor receptor; PBS, phosphate-buffered saline; PNI, peripheral nerve injury; qRT-PCR, quantitative real-time reverse transcription polymerase chain reaction; RCP, recombinant peptide; SFI, sciatic function index; SCs, Schwann cells; SLCs, Schwann-like cells; S100B, S100 calcium-binding protein B; 3D, three-dimensional.

Acknowledgments

We thank Lisa Kreiner, PhD, and H. Nikki March, PhD, from Edanz (https://www.jp.edanz.com/ac) for editing a draft of this manuscript. The graphic abstract was created with BioRender.com.

Authors' Contributions

SC, TI, MS, and YM contributed to the experimental design. SY, SC, OS, and KM performed the data collection, processing, analysis, and interpretation. SC and TT wrote the manuscript. TI and YS contributed to the manuscript revision. All authors read and approved the final manuscript.

Ethical Approval

All animal experiments and procedures were approved by the Animal Care and Use Committee of the University of Tokushima, Tokushima, Japan.

Statement of Animal Rights

All of the experimental procedures involving animals were conducted in accordance with the Institutional Animal Care guidelines of the Animal Care and Use Committee of the University of Tokushima, Tokushima, Japan.

Statement of Informed Consent

There are no human subjects in this article and informed consent is not applicable.

Declaration of Conflicting Interests

The author(s) declared no potential conflicts of interest with respect to the research, authorship, and/or publication of this article.

Funding

The author(s) disclosed receipt of the following financial support for the research, authorship, and/or publication of this article: This study was supported by Grant-in-Aid for Scientific Research, Grant Award Numbers 19K09045 (TI, YM and YS) and 19K09072 (TT and YS).

ORCID iDs

Shuhai Chen https://orcid.org/0000-0003-0734-5848

Tetsuya Ikemoto https://orcid.org/0000-0001-9800-1359

Yu Saito https://orcid.org/0000-0001-6349-1669

References

1. Hoke A. Mechanisms of disease: what factors limit the success of peripheral nerve regeneration in humans? Nat Clin Pract Neurol. 2006;2:448–54.
2. Scheib J, Hoke A. Advances in peripheral nerve regeneration. Nat Rev Neurol. 2013;9:668–76.
3. Pfister BJ, Gordon T, Loverde JR, Kochar AS, Mackinnon SE, Cullen DK. Biomedical engineering strategies for peripheral nerve repair: surgical applications, state of the art, and future challenges. Crit Rev Biomed Eng. 2011;39:81–124.
4. Anderson M, Shelke NB, Manoukian OS, Yu X, McCullough LD, Kumbar SG. Peripheral nerve regeneration strategies: electrically stimulating polymer based nerve growth conduits. Crit Rev Biomed Eng. 2015;43:131–59.
5. Wallis CJD, Peltz S, Byrne J, Kroft J, Karanicolas P, Coburn N, Nathens AB, Nam RK, Hallet J, Satkunasivam R. Peripheral nerve injury during abdominal-pelvic surgery: analysis of the national surgical quality improvement program database. Am Surg. 2017;83:1214–19.
6. Clements MP, Byrne E, Guerrero LFC, Cattin A-L, Zakka L, Ashraf A, Burden JJ, Khadayate S, Lloyd AC, Marguerat S, Parrinello S. The Wound Microenvironment reprograms Schwann cells to invasive mesenchymal-like cells to drive peripheral nerve regeneration. Neuron. 2017;96:98–114.
7. Chen B, Chen Q, Parkinson DB, Dun XP. Analysis of Schwann cell migration and axon regeneration following nerve injury in the sciatic nerve bridge. Front Mol Neurosci. 2019;12:308.
8. Nocera G, Jacob C. Mechanisms of Schwann cell plasticity involved in peripheral nerve repair after injury. Cell Mol Life Sci. 2020;77:3977–89.
9. Xia W, Zhu J, Wang X, Tang Y, Zhou P, Hou M, Li S. ANXA1 directs Schwann cells proliferation and migration to accelerate nerve regeneration through the FPR2/AMPK pathway. FASEB J. 2020;34:13993–4005.
10. Hopf A, Schaefer DJ, Kalbermatten DF, Guzman R, Madduri S. Schwann cell-like cells: origin and usability for repair and regeneration of the peripheral and central nervous system. Cells. 2020;9:1990.

11. Chen S, Ikemoto T, Tokunaga T, Okikawa S, Miyazaki K, Tokuda K, Yamada S, Saito Y, Imura S, Morine Y, Shimada M. Effective in vitro differentiation of adipose-derived stem cells into Schwann-like cells with folic acid supplementation. J Med Invest. 2021;68:347–53.
12. Balakrishnan A, Belfiore L, Chu T-H, Fleming T, Midha R, Biernaskieet J, Schuurmans C. Insights into the role and potential of Schwann cells for peripheral nerve repair from studies of development and injury. Front Mol Neurosci. 2021; 13:608442.
13. He N, Xu Y, Du W, Qi X, Liang L, Wang Y, Feng G, Fan Y, Han Z, Kong D, Cheng Z. Extracellular matrix can recover the downregulation of adhesion molecules after cell detachment and enhance endothelial cell engraftment. Sci Rep. 2015;5:10902.
14. Amer MH, Rose FRAJ, Shakesheff KM, Modo M, White LJ. Translational considerations in injectable cell-based therapeutics for neurological applications: concepts, progress and challenges. NPJ Regen Med. 2017;2:23.
15. Kim EM, Lee YB, Kim SJ, Park J, Lee J, Kim SW, Park H, Shin H. Fabrication of core-shell spheroids as building blocks for engineering 3D complex vascularized tissue. Acta Biomater. 2019;100:158–72.
16. Lin YJ, Lee YW, Chang CW, Huang CC. 3D spheroids of umbilical cord blood MSC-derived Schwann cells promote peripheral nerve regeneration. Front Cell Dev Biol. 2020;8: 604946.
17. Zamproni LN, Mundim MTVV, Porcionatto MA. Neurorepair and regeneration of the brain: a decade of bioscaffolds and engineered microtissue. Front Cell Dev Biol. 2021;9:649891.
18. Ikemoto T, Feng R, Iwahashi S-I, Yamada S, Saito Y, Morine Y, Imura S, Matsuhisa M, Shimada M. In vitro and in vivo effects of insulin-producing cells generated by xeno-antigen free 3D culture with RCP piece. Sci Rep. 2019;9:10759.
19. Wada Y, Ikemoto T, Morine Y, Imura S, Saito Y, Yamada S, Shimada M. The differences in the characteristics of insulin-producing cells using human adipose-tissue derived mesenchymal stem cells from subcutaneous and visceral tissues. Sci Rep. 2019;9:13204.
20. Ohta S, Ikemoto T, Wada Y, Saito Y, Yamada S, Imura S, Morine Y, Shimada M. A change in the zinc ion concentration reflects the maturation of insulin-producing cells generated from adipose-derived mesenchymal stem cells. Sci Rep. 2019; 9:18731.
21. Ikemoto T, Tokuda K, Wada Y, Gao L, Miyazaki K, Yamada S, Saito Y, Imura S, Morine Y, Shimada M. Adipose tissue from type 1 diabetes mellitus patients can be used to generate insulin-producing cells. Pancreas. 2020;49:1225–31.
22. Tokuda K, Ikemoto T, Saito Y, Miyazaki K, Yamashita S, Yamada S, Imura S, Morine Y, Shimada M. The fragility of cryopreserved insulin-producing cells differentiated from adipose-tissue-derived stem cells. Cell Transplant. 2020;29: 963689720954798.
23. Saito Y, Ikemoto T, Tokuda K, Miyazaki K, Yamada S, Imura S, Miyake M, Morine Y, Oyadomari S, Shimada M. Effective three-dimensional culture of hepatocyte-like cells generated from human adipose-derived mesenchymal stem cells. J Hepatobiliary Pancreat Sci. 2021;28:705–15.
24. Nakamura K. CellSaic, a cell aggregate-like technology using recombinant peptide pieces for MSC transplantation. Curr Stem Cell Res Ther. 2019;14:52–56.
25. Lin ZY-C, Hikabe O, Suzuki S, Hirano T, Siomi H, Sasaki E, Imamura M, Okano H. Sphere-formation culture of testicular germ cells in the common marmoset, a small New World monkey. Primates. 2016;57:129–35.
26. Kovalevich J, Langford D. Considerations for the use of SH-SY5Y neuroblastoma cells in neurobiology. Methods Mol Biol. 2013;1078:9–21.
27. Juan C-H, Chen M-H, Lin F-H, Wong C-S, Chien C-C, Chen M-H. In vitro differentiation of human placenta-derived multipotent cells into Schwann-like cells. Biomolecules. 2020;10: 1657.
28. Ho S-Y, Chao C-Y, Huang H-L, Chiu T-W, Charoenkwan P, Hwang E. NeurphologyJ: an automatic neuronal morphology quantification method and its application in pharmacological discovery. BMC Bioinformatics. 2011;12:230.
29. Kim H-S, Lee J, Lee DY, Kim Y-D, Kim JY, Lim HJ, Lim S, Cho YS. Schwann cell precursors from human pluripotent stem cells as a potential therapeutic target for myelin repair. Stem Cell Reports. 2017;8:1714–26.
30. Inserra MM, Bloch DA, Terris DJ. Functional indices for sciatic, peroneal, and posterior tibial nerve lesions in the mouse. Microsurgery. 1998;18:119–24.
31. Nakamura K, Iwazawa R, Yoshioka Y. Introduction to a new cell transplantation platform via recombinant peptide petaloid pieces and its application to islet transplantation with mesenchymal stem cells. Transpl Int. 2016;29:1039–50.
32. Kang Y, Liu Y, Liu Z, Ren S, Xiong H, Chen J, Duscher D, Machens HG, Liu W, Guo G, Zhan P, et al. Differentiated human adipose-derived stromal cells exhibit the phenotypic and functional characteristics of mature Schwann cells through a modified approach. Cytotherapy. 2019;21:987–1003.
33. Frostick SP, Yin Q, Kemp GJ. Schwann cells, neurotrophic factors, and peripheral nerve regeneration. Microsurgery. 1998; 18:397–405.
34. Onode E, Uemura T, Takamatsu K, Yokoi T, Shintani K, Hama S, Miyashima Y, Okada M, Nakamura H. Bioabsorbable nerve conduits three-dimensionally coated with human induced pluripotent stem cell-derived neural stem/progenitor cells promote peripheral nerve regeneration in rats. Sci Rep. 2021;11:4204.
35. Ishihara J, Ishihara A, Fukunaga K, Sasaki K, White MJV, Briquez PS, Hubbell JA. Laminin heparin-binding peptides bind to several growth factors and enhance diabetic wound healing. Nat Commun. 2018;9:2163.
36. Yu CP, Juang JH, Lin YJ, Kuo CW, Hsieh LH, Huang CC. Enhancement of subcutaneously transplanted β cell survival using 3D stem cell spheroids with proangiogenic and prosurvival potential. Adv Biosyst. 2020;4:e1900254.
37. Huang CC, Wei HJ, Lin KJ, Lin WW, Wang CW, Pan WY, Hwang SM, Chang Y, Sung HW. Multimodality noninvasive imaging for assessing therapeutic effects of exogenously transplanted cell aggregates capable of angiogenesis on acute myocardial infarction. Biomaterials. 2015;73:12–22.
38. Bayat N, Ebrahimi-Barough S, Ardakan MMM, Ai A, Kamyab A, Babaloo H, Ai J. Differentiation of human endometrial stem cells into Schwann cells in fibrin hydrogel as 3D culture. Mol Neurobiol. 2016;53:7170–76.
39. Wong CW, Xu Y, Liu X, Xu S, Zhang Y, Zhu Z, He B. Effect of induction time on the proliferation and differentiation of induced Schwann-like cells from adipose-derived stem cells. Cell Mol Neurobiol. 2020;40:1105–16.
40. Kuroda T, Yasuda S, Sato Y. Tumorigenicity studies for human pluripotent stem cell-derived products. Biol Pharm Bull. 2013;36(2):189–92. doi:10.1248/bpb.b12-00970.